Pergamon

Int. J. Solids Structures Vol. 34, No. 4, pp. 461–480, 1997

0020-7683/97 $17.00 + .00

PII: S0020-7683(96)00028-5

STRESS SINGULARITY ANALYSIS IN THREE-DIMENSIONAL BONDED STRUCTURE

HIDEO KOGUCHI
Department of Mechanical Engineering, Nagaoka University of Technology, Kamitomioka 1603-1, Nagaoka, Niigata, Japan 940-21

(*Received* 10 *April* 1995; *in revised form* 31 *January* 1996)

Abstract—Stress analysis for joints between two isotropic materials is performed using three-dimensional boundary element method with Rongved's fundamental solution [Rongved, L. (1955). Force interior to one of two joined semi-infinite solids. In *Second Midwestern Conf. on Solid Mechanics*, pp. 1–13], which satisfies boundary conditions at the interface. The stress distribution around the vertex of the joint is precisely examined and the order of stress singularity obtained in three-dimensional analysis is compared with that in two-dimensional analysis. It is shown that the order of the stress singularity along the stress singularity line, which is the intersection of the interface with the free surface, varies from the value in plane strain to that in plane stress as the opposite side free-surface is approached. The order of stress singularity in the spherical coordinates centered at the vertex is next investigated. When singularity lines with a singularity order meet with each other at the vertex, the order of stress singularity is larger than that for plane strain and plane stress. When the vertex angle between two side free-surfaces is varied, the order of stress singularity is also altered. In particular, a bound at which singularity disappears at the α-β plane for Dundurs' composite parameters is examined for a cubic dissimilar material. It is demonstrated that the bound varies little in comparison with the one obtained from the two-dimensional theory. Copyright © 1966 Elsevier Science Ltd.

1. INTRODUCTION

In recent years, composite materials and metal-ceramic joints have been used widely as industrial materials. Failure in those materials frequently occurs at the edge of joints where the stress concentration rises due to the difference of mechanical properties, and it is deleterious to fracture toughness and reliability of joints. The performance of advanced material systems will be controlled by such highly stressed sites. It is, therefore, important to clarify the characteristics of the stress and displacement fields around the bonded edge. Williams (1952) had investigated the order of stress singularity in a single wedge under various boundary conditions. Bogy (1968, 1970, 1971) had studied the stress singularity near the bonded edges in two-phase materials on the basis of the two-dimensional theory of elasticity. Many investigators [Hein *et al.* (1971), Cook *et al.* (1972), Theocaris (1974), Fenner (1976), Dempsey *et al.* (1979), Barsoum (1988), Pageau *et al.* (1994) and Yang *et al.* (1994)] have examined the behavior of stress singularity around the wedge, edge crack and interface crack. We also have examined the stress field around the apex of joint, and showed in experiment and analysis that the stress concentration in axisymmetric joints could be reduced by varying suitably the edge angle and then the strength of joints could be improved (Koguchi *et al.*, 1994).

Suppose a three-dimensional assembly of dissimilar isotropic materials has several corners as shown in Fig. 1. The three-dimensional asymptotic stress fields around such corners can be studied by considering a polyhedral formed of the free surfaces and the interface. Near the intersection of the interface with the free surfaces, referred to as the vertex, the stress field is in a three-dimensional state. Then, the asymptotic series for the stresses near the vertex can be expressed as follows:

$$r^{\lambda} F_{ij}(\phi, \theta, \lambda) \tag{1}$$

where r is the radial distance from the vertex, ϕ and θ are angles in the spherical coordinates as shown in Fig. 2, and $F_{ij}(\phi, \theta, \lambda)$ is the tensor of angular functions defined on a spherical

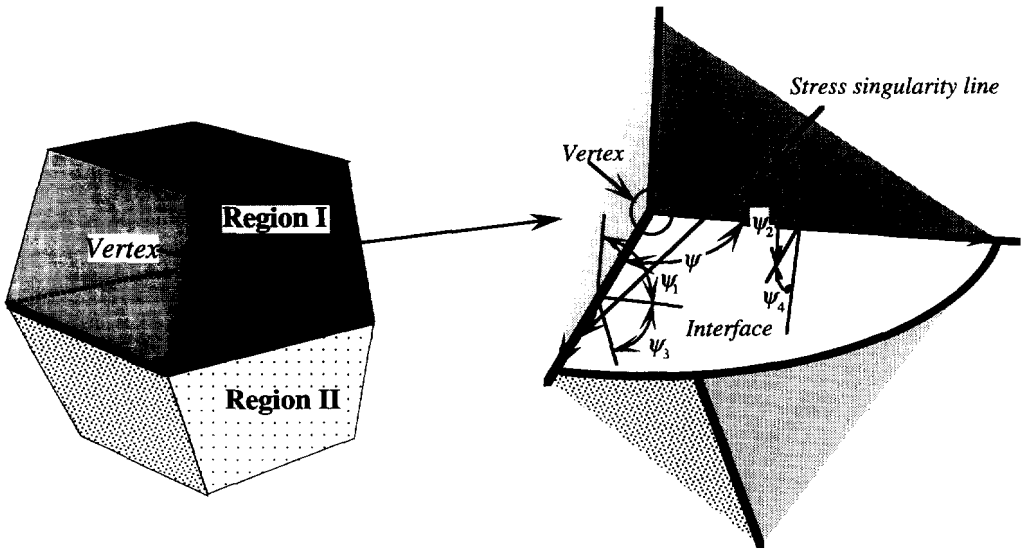

Fig. 1. Stress singularity lines and vertexes at intersection of side free-surfaces with interface in a three-dimensional joint.

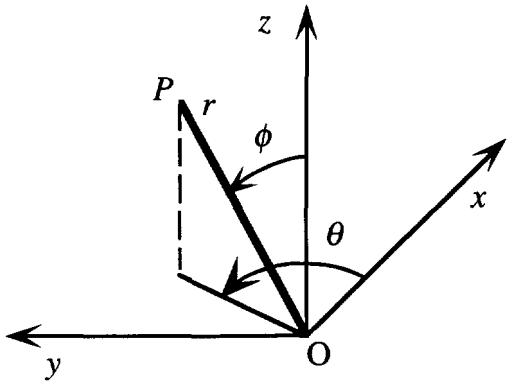

Fig. 2. Spherical coordinates centered at the vertex.

shell of unit radius that surrounds the vertex ($r \to 0$). Corner singularities for homogeneous materials have been investigated by Benthem (1977, 1980), Bazant and Estenssoro (1979), and Ghahremani (1991, 1992). Almost all the studies on the stress singularity treated so far in three-dimensional analyses were concerned with three-dimensional profile cracks. In contrast to the investigation of stress singularity at the crack tip, three-dimensional corner singularity in dissimilar materials has been rarely studied. A recent paper by Pageau and Biggers (1995) considers the three-dimensional intersection of a multi-material junction with a free surface. In the present study, the stress singularity occurs not only at the vertex but also along the intersection of the interface with the free surface, and we refer to the cross line as the stress singularity line. There are usually several stress singularity lines in actual bonded structures. Incidentally, as shown in Fig. 1, the vertex is a cross point of four free surfaces with the interface: a point crossing two stress singularity lines with different order of stress singularity. The stress field around such a vertex of a joint has not been so far clarified, for instance, when a line with a stress singularity meets one without a singularity and so on. We do not know well whether many results concerning dissimilar materials in two-dimensional analyses can be employed to actual three-dimensional joints. In this paper, we first report the stress field around a vertex in cases where (1) two singularity lines with the same singularity meet each other, (2) a line with singularity meets one without singularity, and (3) two lines without singularity meet. An influence of variation of vertex angle ψ (see Fig. 1) upon the order of stress singularity is next investigated. Here, when the angle, ψ, between two side free surfaces is varied while holding a relation of edge angles

$\psi_1 = \psi_2 = \psi_3 = \psi_4 = 90^\circ$ fixed, it is examined whether the order of stress singularity varies with the angle, which cannot be taken into account in the two-dimensional analysis. Finally, a bound of material combinations on α-β Dundurs' parameters plane yielding no stress singularity at the vertex is investigated (Dundurs, 1969), α and β are defined as follows:

$$\alpha = \frac{\kappa m_{II} - m_I}{\kappa m_{II} + m_I}$$
$$\beta = \frac{\kappa(m_{II} - 2) - (m_I - 2)}{\kappa m_{II} + m_I} \tag{2}$$

where

$$\kappa = \frac{G_I}{G_{II}}, \tag{3}$$

$$m = \begin{cases} 4(1-\nu) & \text{for plane strain} \\ \dfrac{4}{1+\nu} & \text{for plane stress} \end{cases} \tag{4}$$

in which G is shear modulus and ν is Poisson's ratio. Subscripts in these parameters represent the region of materials: I refers to the upper region and II the lower region in Fig. 1.

2. CHARACTERISTICS OF STRESS DISTRIBUTION NEAR THE VERTEX

Thompson *et al.* (1970) investigated the order of stress singularity at the end of a cone on the basis of three-dimensional theory of elasticity. After that, the order of stress singularity at the cross point of free surface with crack front in a three-dimensional shape crack was intensively examined by Bazant and Estenssoro (1979), Benthem (1977, 1980), and Ghahremani (1991, 1992) using the principle of minimum potential energy, three-dimensional theory of elasticity, variational principle and so on. In contrast to these studies, it seems that three-dimensional stress analyses for bonded structure with a general configuration have not been so far performed. Recently, Pageau and Biggers (1995) investigated the three-dimensional intersection of multi-material junction by using FEM with a singular element.

To examine the stress singularity at the vertex of a joint, a spherical coordinate system with the origin at the cross point of singularity lines is introduced as follows (see Fig. 2):

$$\begin{cases} x = r\sin\phi\cos\theta \\ y = r\sin\phi\sin\theta \\ z = r\cos\phi \end{cases} \tag{5}$$

Then, the stress components in the coordinate system can be expressed as the following asymptotic series,

$$\sigma_{ij} = \sum_{k=1} r^{\lambda_k} F_{ij}^k(\phi, \theta, \lambda_k) \tag{6}$$

where λ_k is the kth eigenvalue determined from the boundary condition,

$$\lambda_1 < \lambda_2 < \cdots < \lambda_n < \cdots$$

where $-1 < \lambda_k < 0$, the stress field has a singularity, and $F_{ij}^k(\phi, \theta, \lambda_k)$ is the intensity of the stress fields. Then, the stress components can be arranged as follows:

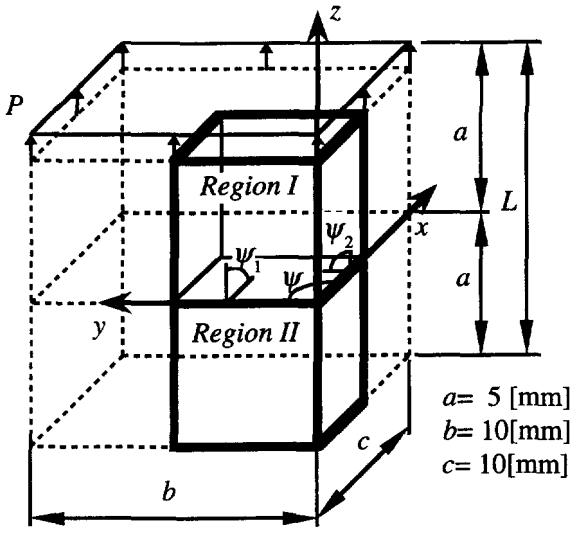

Fig. 3. Typical model of joint for analysis and Cartesian coordinates. Size of L, a and b are common for other joints with varied edge angles ψ_1, ψ_2 and ψ.

$$\sigma_{ij} = r^{\lambda_1} F_{ij}^1(\phi, \theta, \lambda_1)\left\{1 + r^{\lambda_2-\lambda_1}\frac{F_{ij}^2}{F_{ij}^1} + r^{\lambda_3-\lambda_1}\frac{F_{ij}^3}{F_{ij}^1} + \cdots\right\}. \tag{7}$$

When the radial distance from the vertex, r, is sufficiently small, the second and subsequent terms are approximated to zero, because of $\lambda_2-\lambda_1 > \lambda_3-\lambda_1 > \cdots > 0$. Here, the stress near the vertex is investigated at r so small that the plots of stress distribution against r become straight in a log-log scale. In such a case, (7) agrees with (1).

2.1. *Stress analysis of bonded structures*

We must pay attention to the mesh division to examine precisely the stress distribution of the portion including the stress concentration using FEM or BEM. Particularly, in the calculation of three-dimensional FEM for a complex structure, a vast memory for large numbers of elements is needed to obtain the stress distribution in the structure. On the other hand, three-dimensional BEM is useful to analyze efficiently the stress fields in such a structure from the views of preparation of mesh data, since only surfaces are divided into mesh for analysis. BEM will be able to calculate accurately the stress and displacement fields for any points in the joint with highly stressed sites by preparing fine mesh data.

The boundary integral equation in terms of the displacement vector, $\mathbf{u}_j$, and traction vector, $\mathbf{t}_j$, can be expressed as follows:

$$C_{ij}\mathbf{u}_j(P) = \int_S \{U_{ij}(P, Q)\mathbf{t}_j(Q) - T_{ij}(P, Q)\mathbf{u}_j(Q)\}\, \mathrm{d}S(Q) \tag{8}$$

where P and Q are points on the boundary, C_{ij} are constants determined from the configuration of boundary, U_{ij} and T_{ij} are the fundamental solutions for displacement and surface traction, respectively.

Equation (8) is discretized using a quadrilateral serendipity element and a simultaneous equation for unknown variables is derived. By the way, in a previous paper (Li *et al.*, 1992), we reported the results of the stress analyses for dissimilar materials using three-dimensional boundary element method with Kelvin's fundamental solution. When the ordinal Kelvin's fundamental solution is employed in the analysis of joints, their interface must be also divided using finer meshes at the vertex of joints and along the stress singularity lines. Then, huge memory and time consuming analyses are required for accurately analyzing the stress fields. In the present study, Rongved's fundamental solution satisfying the boundary condition at the interface is, therefore, employed (see Appendix).

A typical model employed in our calculation is shown in Fig. 3, where every free surface is a square of the same size, a side of which is 10 mm in length and the interface of

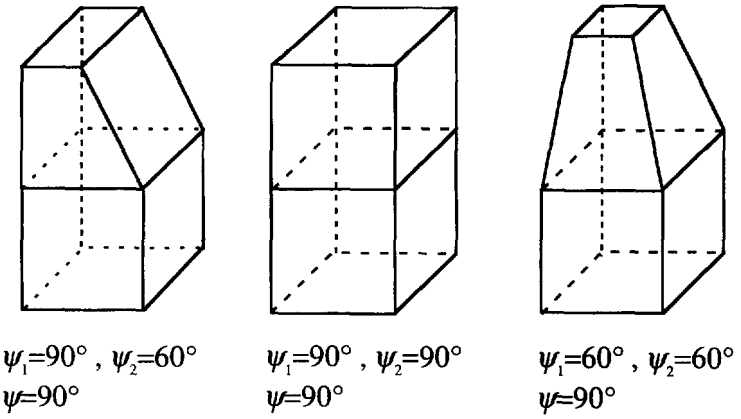

Fig. 4. Three models of joint with varied edge angles, ψ_1 and ψ_2.

joint is at the middle of the upper and the lower surfaces. Several models with different edge angles, ψ_1 and ψ_2, of region I, as shown in Fig. 3, are first analyzed under a pair of elastic moduli of two materials. The analyses are performed under the condition where a uniform constant tensile stress, $\sigma_{zz}(=P)$, is applied at the upper surface and the displacement in the z-direction only at the lower surface is fixed. The edge angles in the region II are fixed to a right angle and those of region I are modified to (1) $\psi_1 = \psi_2 = \psi = 90^\circ$, (2) $\psi_1 = \psi = 90^\circ$, $\psi_2 = 60^\circ$ and (3) $\psi_1 = \psi_2 = 60^\circ$, $\psi = 90^\circ$ as shown in Fig. 4.

2.2. *Estimation of order of stress singularity near the vertex*

Before proceeding to three-dimensional analysis, the procedure estimating the order of stress singularity by BEM adopted here will be described. The order is obtained from the estimation of the slope of log-log plot of the stress distribution at the neighborhood of the vertex. The value of order may vary with coarseness of mesh, and a known value of order in two-dimensional joints is here compared with the numerical one. Now we consider a joint with apex angles, γ' and γ'', as shown in Fig. 5. A schematic view and mesh division

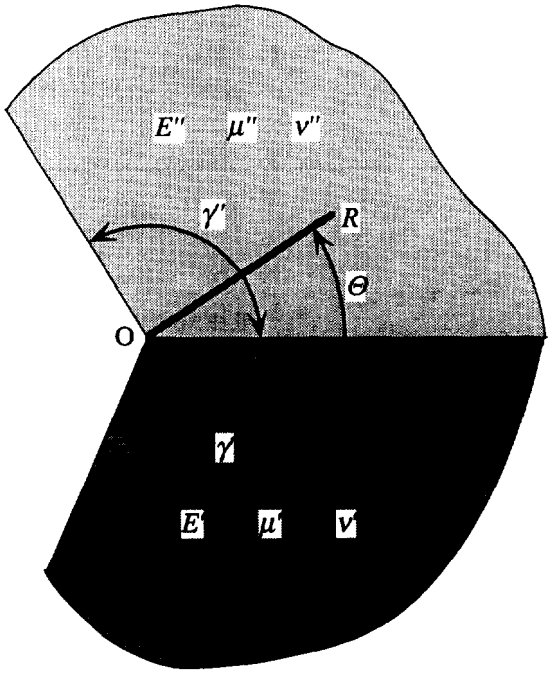

Fig. 5. Description of parameters for two-dimensional joint.

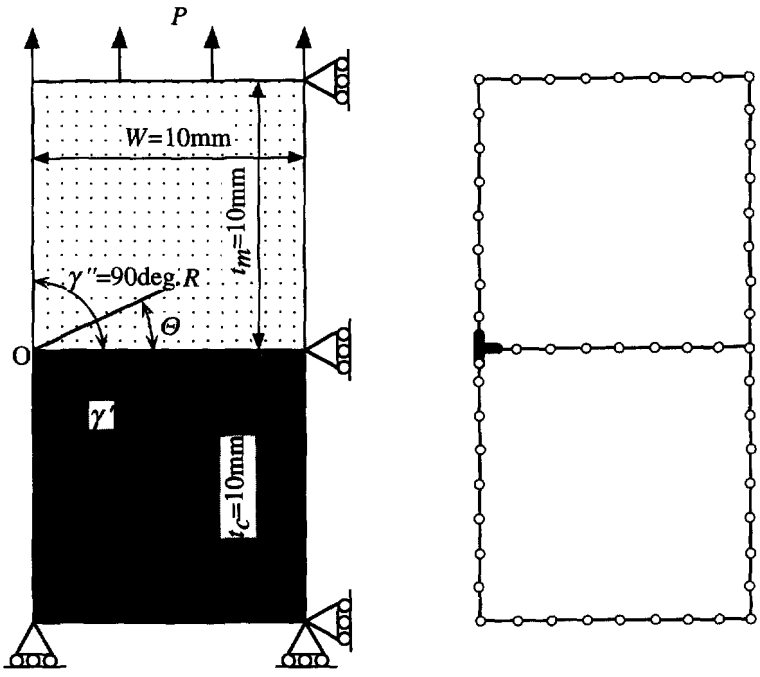

Fig. 6. Typical model of joint and mesh division for two-dimensional analysis. Load is applied on upper edge.

of two-dimensional joints for analysis are shown in Fig. 6. Kelvin's fundamental solution in two-dimensional elasticity and a quadratic serendipity element are used in the analysis. A rectangular joint of being 20 mm in length and width is analyzed as a standard model, and the numbers of element and node for the model are 100 and 200, respectively. A minimum length of an element around the vertex is 0.1 μm. The stress distribution in a joint composed of elasticity moduli, $E' = 100$ GPa, $\nu' = 0.37$, $E'' = 340$ GPa and $\nu'' = 0.25$, is first analyzed and the results of stress distribution in plane strain are shown in Fig. 7 for several angles, Θ. This log-log plot for stress, $\sigma_{\Theta\Theta}$, yields straight lines with the same slope for every angle and the stress increases with approaching the vertex, $R \to 0$. For this case, the order of stress singularity is derived from Bogy's eigenequation as -0.1226 in plane strain and -0.0925 in plane stress. The mean value of slope obtained by using least square method for all plots is -0.1227, and this value agrees well with theoretical one. The slopes

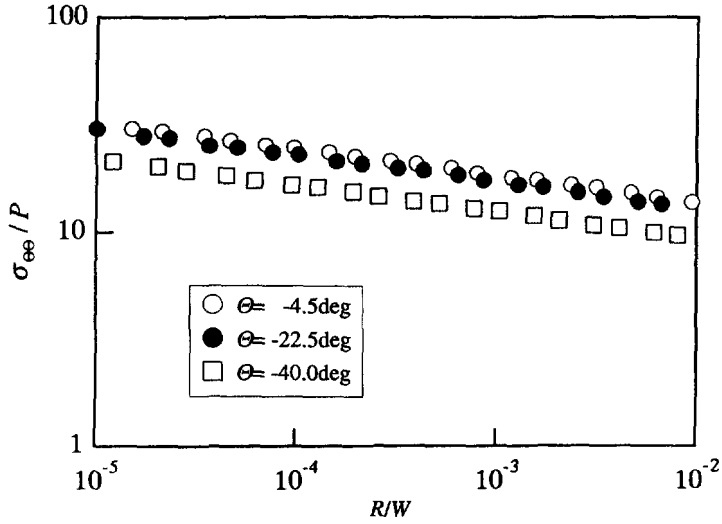

Fig. 7. Distribution of dimensionless stress, $\sigma_{\Theta\Theta}/P$ against R/W for several angles, Θ.

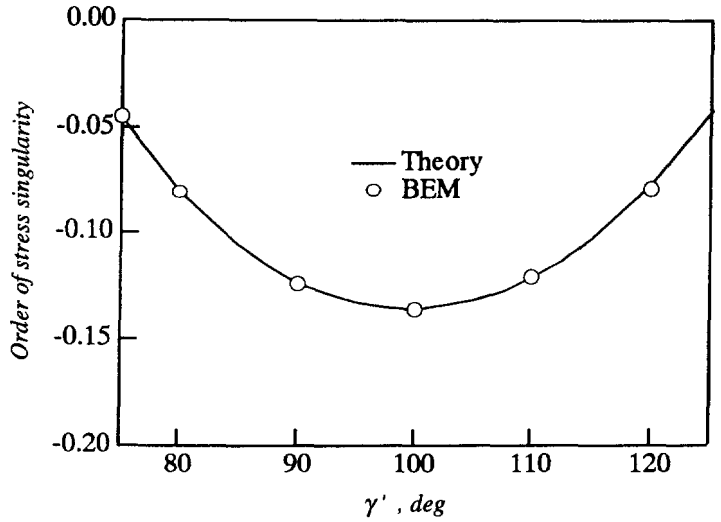

Fig. 8. Variation of singularity order with apex angle, γ', under the condition of $\gamma'+\gamma'' = 180^\circ$. Comparison of results obtained by the theory of two-dimensional elasticity and the two-dimensional BEM.

for other stress components, σ_{RR} and $\sigma_{R\Theta}$, are agreed with each other within 0.86% error, and the plot becomes straight line with the same slope within $R/W < 10^{-2}$, where R is a distance from the vertex. Furthermore, the order of stress singularity for joints varying the vertex angle like as $\gamma'+\gamma'' = 180$ degrees is examined using the same minimum length of element and material combination as before. Results of order estimated by BEM and Bogy's theory are shown in Fig. 8 against the vertex angle, γ'. Solid line and open dots represent theory and BEM, respectively. Both results are agreed with each other.

We will examine next the order of stress singularity in three-dimensional joints on the basis of the results of two-dimensional analyses. It is known that when the configuration of an element becomes slender and irregular, the accuracy of analysis reduces. If such an element is assembled along the stress singularity line, significant errors may be caused in the results of the analysis. So, a triangular element constructed by degenerating two nodes in a quadrilateral element into one is employed at a portion changing gradually the mesh size along the singularity line. Parts indicated by bold solid lines as depicted in Fig. 3 are divided into a mesh utilizing the symmetry of joint configuration. As mentioned before, a quadratic triangular element is employed for analyzing accurately the stress field along the singularity line and near the vertex. An example of mesh division for the joint with angles $\psi_1 = \psi_2 = \psi_3 = 90^\circ$ is shown in Fig. 9, where a minimum length of an element at the vertex is 0.03 μm, the total number of elements is 482 and the total number of nodes is 1063. The stress fields are here computed by setting $E_1 = 100$ GPa, $E_2 = 500$ GPa, $\nu_1 = 0.37$ and $\nu_2 = 0.25$. Then, the stress singularity does not occur at the edge angle of 60° in plane stress and in plane strain. The stress singularity occurs at the edge angle more than 65° in plane strain and 72° in plane stress under this pair of materials. The orders of stress singularity for these pairs of edge angles are presented in Table 1.

Figure 10 shows a log-log plot of stress, σ_{zz}, non-dimensionalized by the applied stress P on the upper surface of joint. The plotted values are the ones on the interface at the distance, r_y, from the free surface along the y-coordinate axis, and the axis of abscissa is the dimensionless value of the distance, r_x, from the free surface divided by a representative length, L, of the joint. We can see from this figure that the plots are almost linear in a log-log scale and their slopes are negative. These results mean that the stress fields near the vertex have a singularity. Figure 11 shows the variation of the order of stress singularity with the dimensionless distance, r_y/L. The order varies from the one in plane strain to that in plane stress as the position of plot approaches to the free surface, and it may become slightly less than the one in plane stress very near the free surface. Here the value of stress singularity is -0.13 in plane stress and -0.169 in plane strain, respectively.

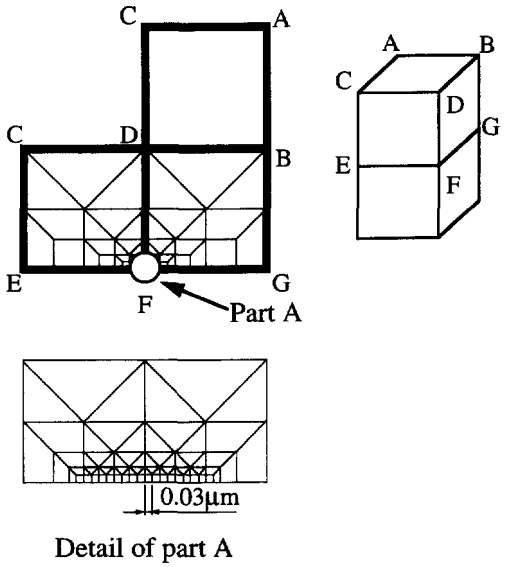

Fig. 9. An example of global mesh division and mesh near the vertex for typical model of joint.

Table 1. Material properties and order of stress singularity

Region	Young's modulus E [GPa]	Poisson's ratio ν	Apex angle [degree]	Order of stress singularity	
				Plane strain	Plane stress
I	100	0.37	90		
II	500	0.25	90	−0.169	−0.13
I	100	0.37	60		
II	500	0.25	90	0.070	0.28

2.3. *The order of stress singularity and stress distribution in spherical polar coordinate system near the vertex*

Figure 12 demonstrates the distributions of several stress components, σ_{rr}, $\sigma_{r\phi}$, $\sigma_{\phi\phi}$ and $\sigma_{\theta\theta}$ on the interface against the distance, r, from the vertex in spherical polar coordinate system (see Fig. 2). Results plotted in this figure are those at different angles, ϕ and θ, taken from the polar and the side free-surface. Slope of each line in a log-log scale is the same value, $\lambda = -0.208$, which is approximately 1.6 times as large as that in plane stress. Thus, when two singularity lines with the same order of singularity meet at the vertex, it is found that the order of stress singularity yielded in a three-dimensional polar coordinate system becomes larger than that yielded in two-dimensional one. If the intersection of free surface with the interface produces a stress singularity line, the possibility that failure occurs at the vertex becomes considerably higher than on the singularity line.

When the edge angles, ψ_1 and ψ_2, are 90° and 60°, the distributions of normal stress, σ_{zz}, on the interface are shown in Figs 13 and 14 versus distances, r_x and r_y, respectively, from the side free surfaces. The former is the variation of the distribution with the distance from the free surface along the y-axis, and the latter is the one along the x-axis. The stress singularity, an apparent mean order estimated by using the least squares method within $r_x/L \leqslant 10^{-4}$ is $\lambda = -0.174$, and still exists at the free surface with the apex angle of 90°. These plots have a slight curvature as $r_y/L \to 0$, owing to the decrease of accuracy of calculation. When an inner point approaches the free surface on the interface, the stresses at the point are more influenced by the oblique free surface with an apex angle of 60° than the free surface with an angle of 90°, since the point is closer in the oblique surface than in the perpendicular surface to the free surface. On the contrary, the singularity at the free surface with an apex angle of 60° diminishes and the slope of lines in a log-log plot obtained by using least square method for $r_y/L \geqslant 9.0 \times 10^{-5}$ is approximately 0.193. We need, furthermore, a small element size and mesh division when the stresses developed in rectangular

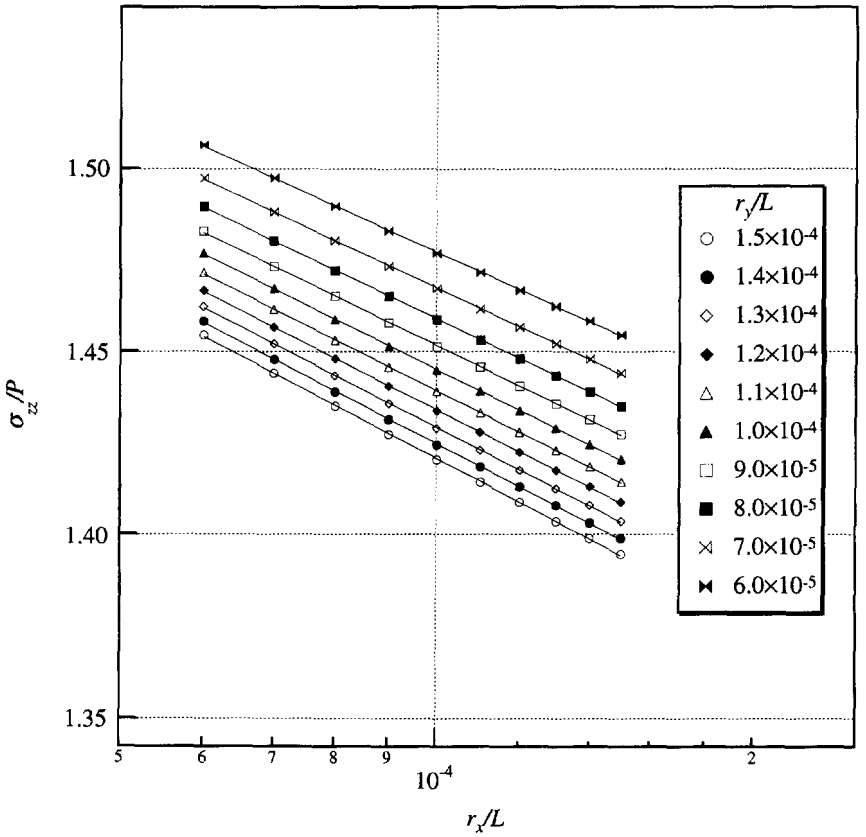

Fig. 10. The distribution of dimensionless stress σ_{zz}/P against the dimensionless distance, r_x/L, from side free-surface in the direction of x-axis. The apex angles are $\psi_1 = 90^\circ$, $\psi_2 = 90^\circ$ and $\psi = 90^\circ$.

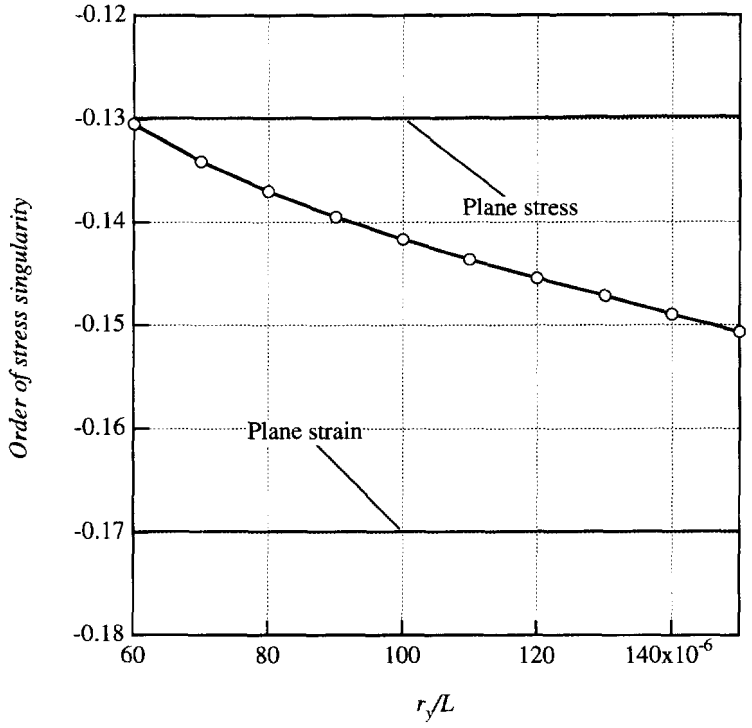

Fig. 11. Variation of the order for stress singularity with distance from the free-surface.

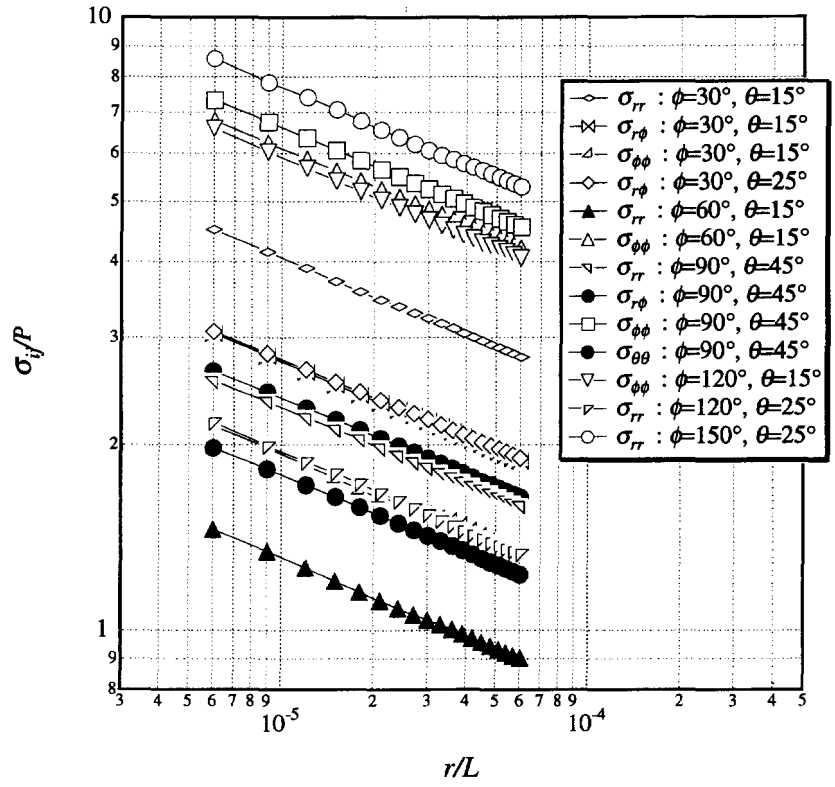

Fig. 12. Distribution of dimensionless stresses, σ_{ij}/P, against r/L for several angles θ and ϕ. The apex angles are $\psi_1 = 90°$, $\psi_2 = 90°$ and $\psi = 90°$.

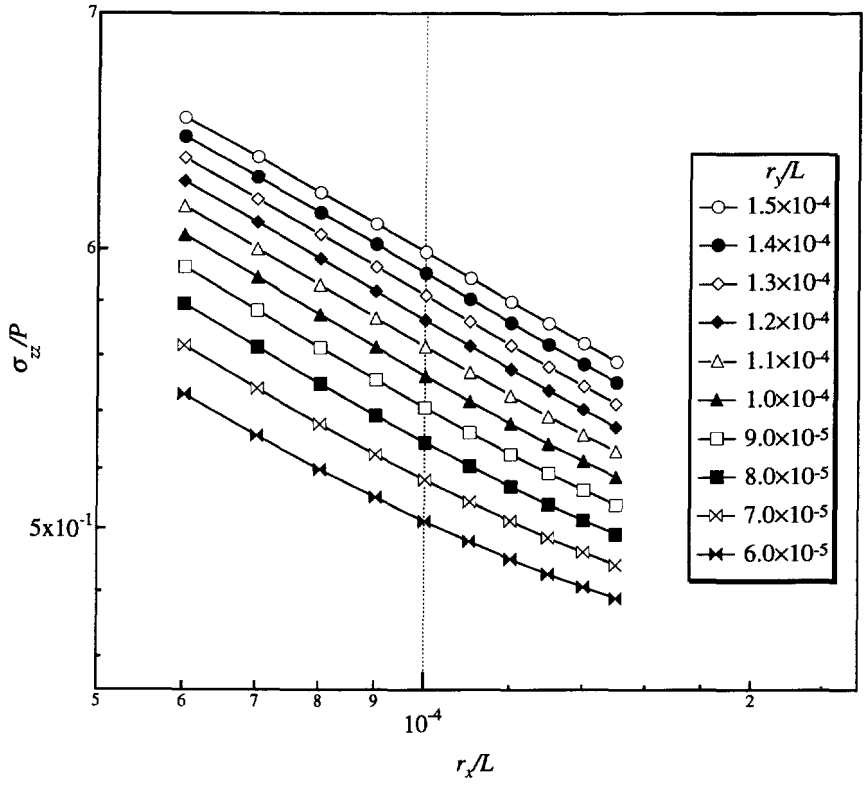

Fig. 13. Distribution of dimensionless stress, σ_{zz}/P, on the interface against r_x/L. The apex angles are $\psi_1 = 90°$, $\psi_2 = 60°$ and $\psi = 90°$.

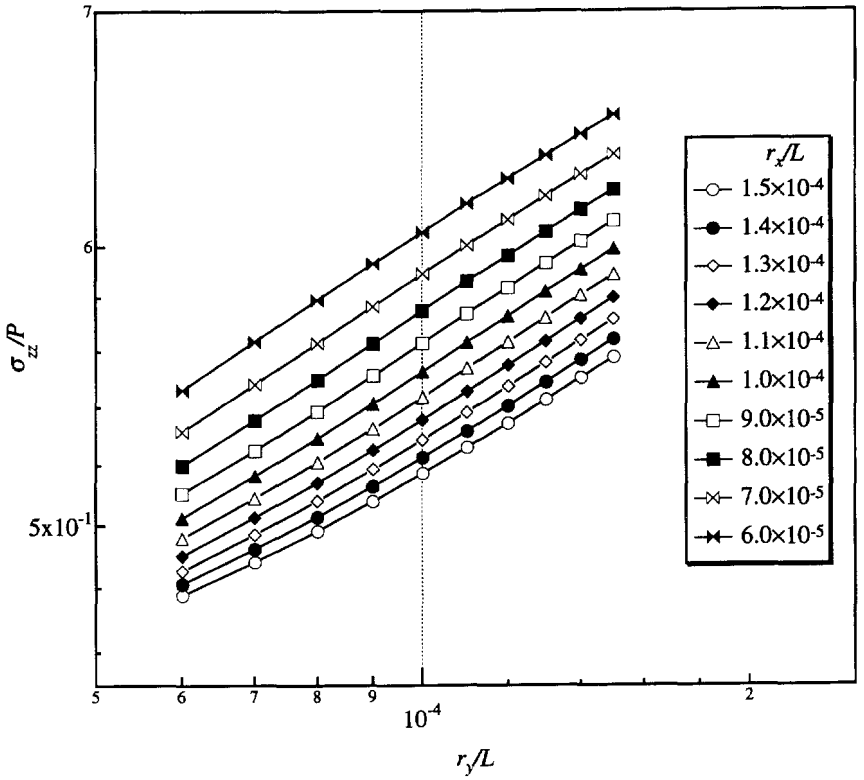

Fig. 14. Distribution of dimensionless stress, σ_{zz}/P, on the interface against r_y/L. The edge angles are $\psi_1 = 90^\circ$, $\psi_2 = 60^\circ$ and $\psi = 90^\circ$.

coordinates by varying the apex angle do not have a stress singularity. We thus suppose that the stress distributions in this joint are complicated near the vertex. Figure 15 demonstrates the distribution of stress, $\sigma_{\phi\phi}$, on the interface against r/L at several angles, θ, which measured from the free surface with the apex angle of 60°. The plot for $\theta = 15^\circ$ is at the nearest position to the free surface with apex angle of 60°, and its magnitude is extremely small. The value of the plot decreases approaching the origin owing to the disappearance of stress singularity at the side free-surface with apex angle of 60°. As to the angle $\theta = 75^\circ$, the stress level is extremely high, but it decreases approaching the origin owing to the influence of the free surface with no singularity. The magnitude of stress in this joint becomes extremely small in comparison with that in the joint with edge angles 90° and −90°. The mean singularity order for these plots is about 0.038. This means that the stress concentration at the vertex in the three-dimensional joint can be also reduced if the singularity for one of the side free-surfaces vanishes.

Figure 16 shows the distribution of stress, σ_{zz}, on the interface against r_x/L in the joint with the apex angles $\psi_1 = \psi_2 = 60^\circ$. The abscissa in this figure is the dimensionless distance from the free-surface along the x-axis and the ordinate is the dimensionless stress, σ_{zz}/P. It is found that the plots have a slight curvature in a log-log scale and the stress singularity vanishes at the vertex, since the slope of the plots is positive; approximately 0.137 using least square method for all plots. As previously mentioned, a calculation with a high accuracy for the stress distribution in rectangular coordinate system requires a smaller element size and a greater number of elements. Figure 17 represents the distribution of stress, $\sigma_{\phi\phi}$ on the interface of a joint, against the distance from the vertex. The lines plotted for several different angles, θ, have slightly different slopes, the mean value of which, obtained by using least squares method, is approximately 0.27, and the value is approximately twice as large as that for the lines shown in Fig. 16.

In this section, we show that even when the pair of materials yields the stress singularity at the vertex of a joint, the stress singularity can be diminished by adequately varying the apex angle of the joint, and the calculation for an exact stress distribution in a plane

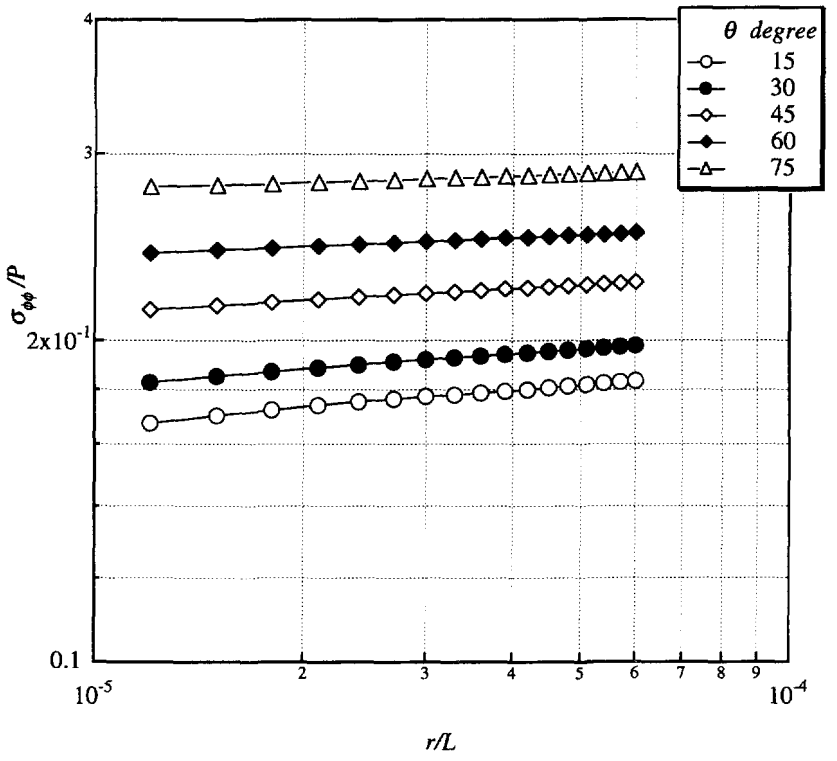

Fig. 15. Distribution of dimensionless stress, $\sigma_{\phi\phi}/P$, on the interface against r/L for several angles θ. The apex angles are $\psi_1 = 90^\circ$, $\psi_2 = 60^\circ$ and $\psi = 90^\circ$.

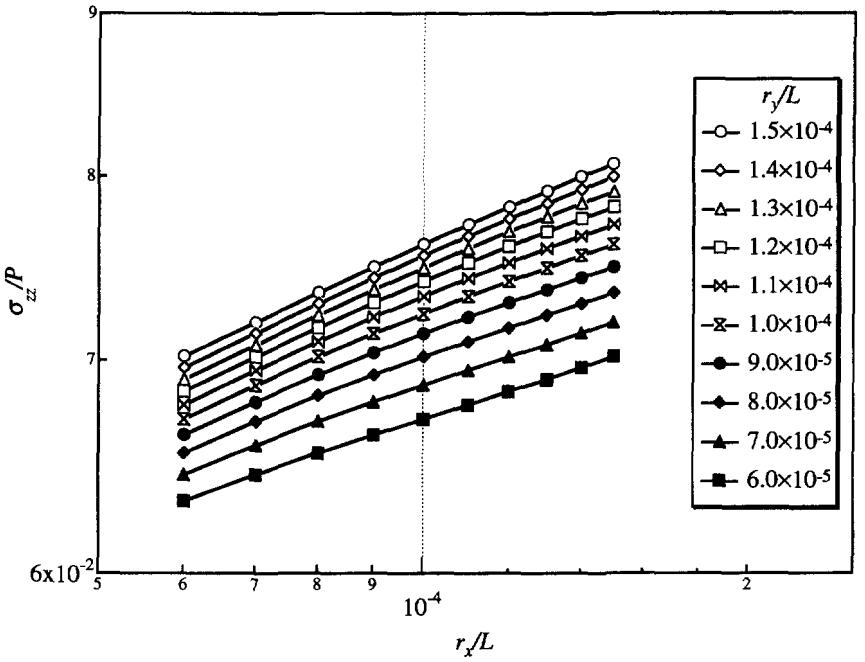

Fig. 16. Distribution of dimensionless stress, σ_{zz}/P, on the interface against r/L. The apex angles are $\psi_1 = \psi_2 = 60^\circ$ and $\psi = 90^\circ$.

extremely close to the side free surface requires a finer mesh and a greater number of elements. So, the apex angles of the side free surface are fixed at $\psi_1 = \psi_2 = 90^\circ$ in the stress analysis carried out in the next section.

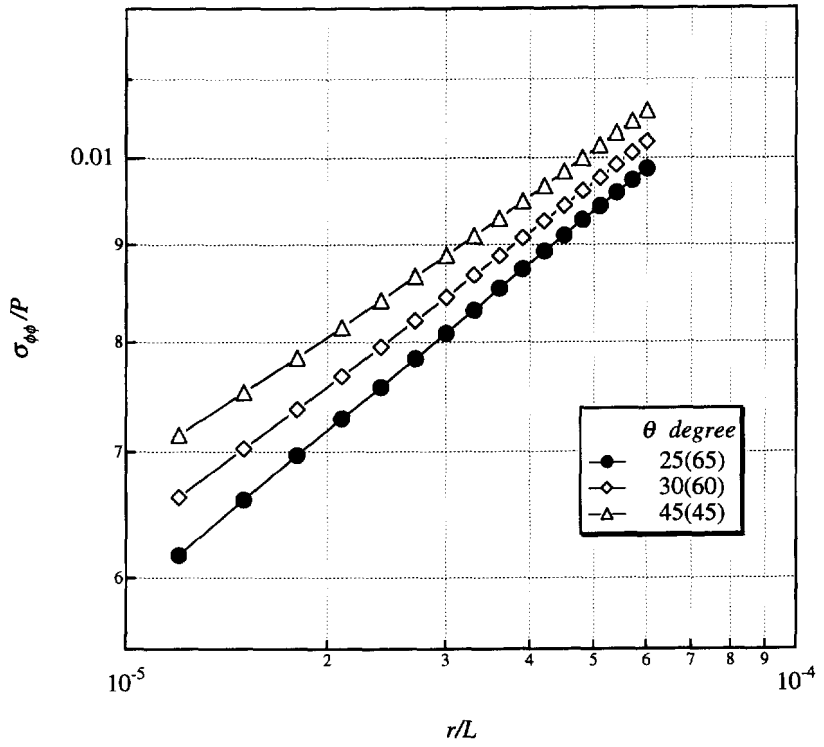

Fig. 17. Distribution of dimensionless stress, $\sigma_{\phi\phi}/P$, on the interface against r_s/L for several angles θ. The edge angles are $\psi_1 = \psi_2 = 60°$ and $\psi = 90°$.

Table 2. Materials parameters used in calculation

Value of Dundurs' parameters in plane strain			Order of stress singularity		Material properties			
					E [GPa]		ν	
No.	α	β	plane strain	plane stress	I	II	I	II
1	0.507	0	−0.15	−0.118	100.0	27.5	0.15	0.422
2	0.612	0	−0.20	−0.154	100.0	19.99	0.2	0.450
3	0.713	0	−0.25	−0.187	100.0	14.26	0.3	0.475
4	0.809	0	−0.30	−0.231	100.0	8.34	0.15	0.477
5	0.902	0	−0.35	−0.270	100.0	3.96	0.1	0.488

2.4. *Order of stress singularity in varying the vertex angle between two side free-surfaces*

When the apex angle of the three-dimensional joint was altered, the order of stress singularity at the vertex varied much more than the value of the order estimated from the two-dimensional theory of elasticity. Furthermore, it is supposed that it may be possible to vary the order of singularity at the vertex in a three-dimensional stress state by changing the vertex angle, ψ, between side free-surfaces. The influence of variation with the angle, ψ, upon the order of singularity has never been elucidated. When the combination of materials and edge angles (ψ_1, ψ_2, ψ_3 and ψ_4 shown in Fig. 1) of the joint are fixed, a notable variation of the order may not be expected, because it is considered that the stress singularity originates from the difference of material properties and the edge angles. To examine this point, we perform stress analyses for the joint with edge angles $\psi_1 = \psi_2 = \psi_3 = \psi_4 = 90°$, following the results of the previous section under several pairs of material properties. The pairs of materials employed in this calculation are shown in Table 2. The pairs of α and β in plane strain are plotted on the Dundurs' composite parameter plane as shown in Fig. 18. The order of singularity estimated on the basis of the two-dimensional theory of elasticity for these material pairs is also noted in Table 2. You can see that the order in

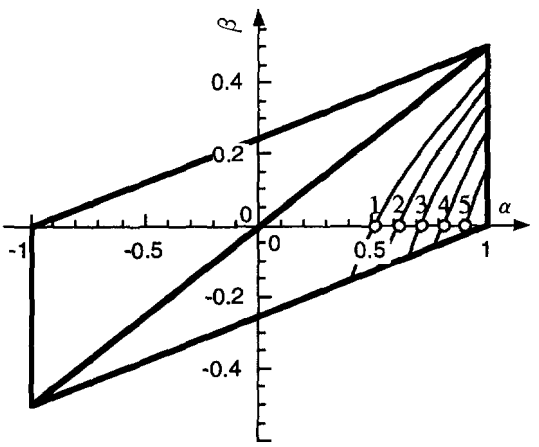

Fig. 18. Pairs of Dundurs' composite parameters examined the order of stress singularity in plane strain. The apex angles $\psi_1 = \psi_2 = \psi_3 = \psi_4 = 90^\circ$.

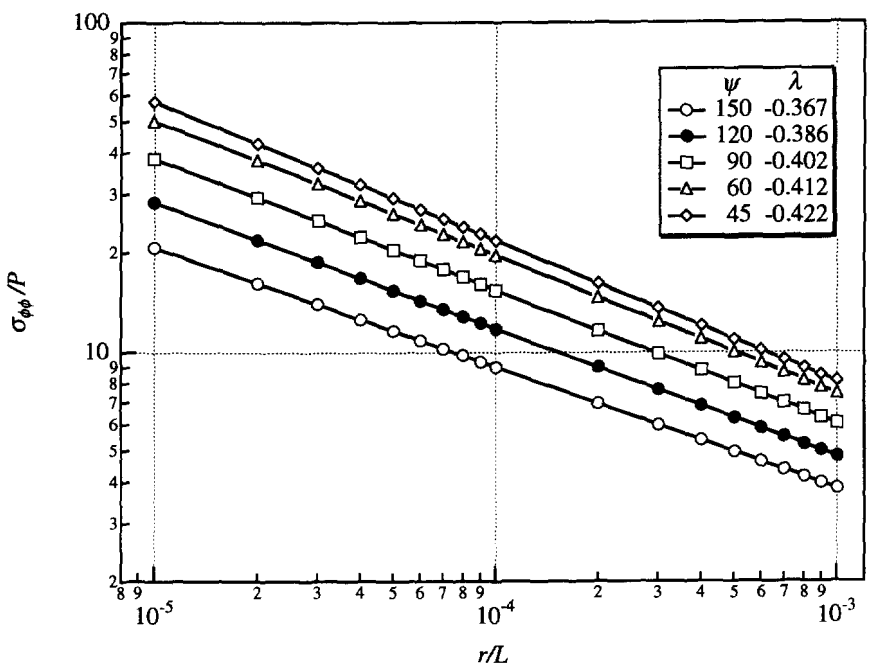

Fig. 19. An example of distribution of dimensionless stress, $\sigma_{\phi\phi}/P$, at $\theta = 45^\circ$ on the interface for several angles, ψ. ($\alpha = 0.902$ and $\beta = 0$.)

plane strain varies in an orderly way, although the one in plane stress does not always change regularly owing to the difference of the definition of m and κ. Here, when the vertex angles, ψ, between two side free surfaces are 45°, 60°, 90°, 120° and 150°, the order of stress singularity in the spherical coordinate system is investigated. Figure 19 is an example of the distribution of stress, $\sigma_{\phi\phi}$ at $\theta = 45^\circ$ on the interface in $\alpha = 0.902$ and $\beta = 0$, and the plotted lines were almost straight in all the cases of the angle ψ. The order of singularity increases with the decrease of the vertex angle, ψ. We can say that failure of joints, therefore, occurs more easily in those with a smaller vertex angle.

We investigate how large the order λ in the spherical coordinate system is in comparison with the order $\lambda_{plane\ stress}$ in plane stress. Figure 20 demonstrates the relationship between the ratio of λ to $\lambda_{plane\ stress}$ and the order $\lambda_{plane\ strain}$ in plane strain. The ratio in a large vertex angle is always smaller than that in a small one. The ratio of $\lambda_{plane\ strain}$ to $\lambda_{plane\ stress}$ is also added to this figure. We can see that, when the vertex angle ψ increases, the variation of $\lambda/\lambda_{plane\ stress}$ with $\lambda_{plane\ strain}$ behaves in a way similar to that of the ratio $\lambda_{plane\ strain}/\lambda_{plane\ stress}$. The value of the ratio $\lambda_{plane\ strain}/\lambda_{plane\ stress}$ seems to agree with a fixed value corresponding to each vertex

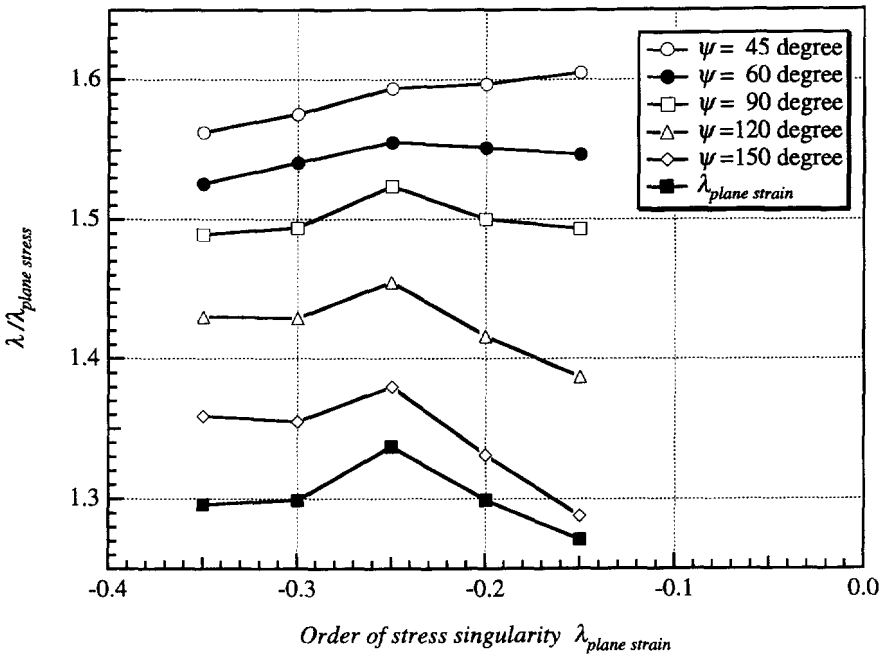

Fig. 20. Relationship of the ratio of λ to $\lambda_{plane\ stress}$ and against $\lambda_{plane\ strain}$.

angle. The order of stress singularity in the spherical coordinate system depends not only on the combination of materials and edge angles but also on the vertex angle between two side free-surfaces.

2.5. *Bound yielding no stress singularity on Dundurs' composite plane*

It was shown in Section 2.2 that the order of stress singularity at the vertex of a joint was different from that estimated by the two-dimensional analysis and varied for material combinations. It is, therefore, supposed from this fact that the bound yielding no stress singularity on Dundurs' composite parameter plane is unlike one obtained from the two-dimensional theory of elasticity. Hence, we perform a stress analysis for the joint with angles $\psi_1 = \psi_2 = \psi_3 = \psi_4 = \psi = 90^\circ$ to examine the bound that the stress singularity disappears under several pairs of Dundurs' parameters.

As shown by the bold solid line on Dundurs' composite plane in Fig. 21, we investigate the pairs yielding no stress singularity by varying either α at fixed β or β at fixed α in the direction indicated by arrows. Figure 22(a) and (b) are examples of stress distributions for several values of β at $\alpha = 0.8$ and for several values of α at $\beta = -0.225$. The bound diminishing the singularity is here considered to be the pair of α and β yielding a value of λ whereby the first 4 digits are zero. Figure 23 represents Dundurs' α-β plane plotting the bound vanishing the stress singularity at the vertex. Dotted lines drawn in this figure represent the bound in which the parameters α and β exists in plane stress. It is found that the bound vanishing the stress singularity in a three-dimensional stress state varies little compared to that in the two-dimensional theory, nevertheless the order of stress singularity changes greatly within the domain incurring the singularity on the Dundurs' α-β plane. Precisely, the bound shifts slightly within the overlapped domain of the α-β plane in plane strain and plane stress. It moves a little into the domain yielding stress singularity in plane strain and out of the domain yielding it in plane stress. The condition yielding no singularity in plane strain and in plane stress is satisfied within a common domain, although it is satisfied only in plane strain at the outside of the common domain. Consequently, it is considered that the bound yielding no singularity shifts at the outside of the overlapped domain owing to non-satisfaction of the condition yielding no singularity in plane stress. The present results suggest that the stress concentration occurring in dissimilar materials can be reduced by applying the results of the two-dimensional analysis in manufacturing any

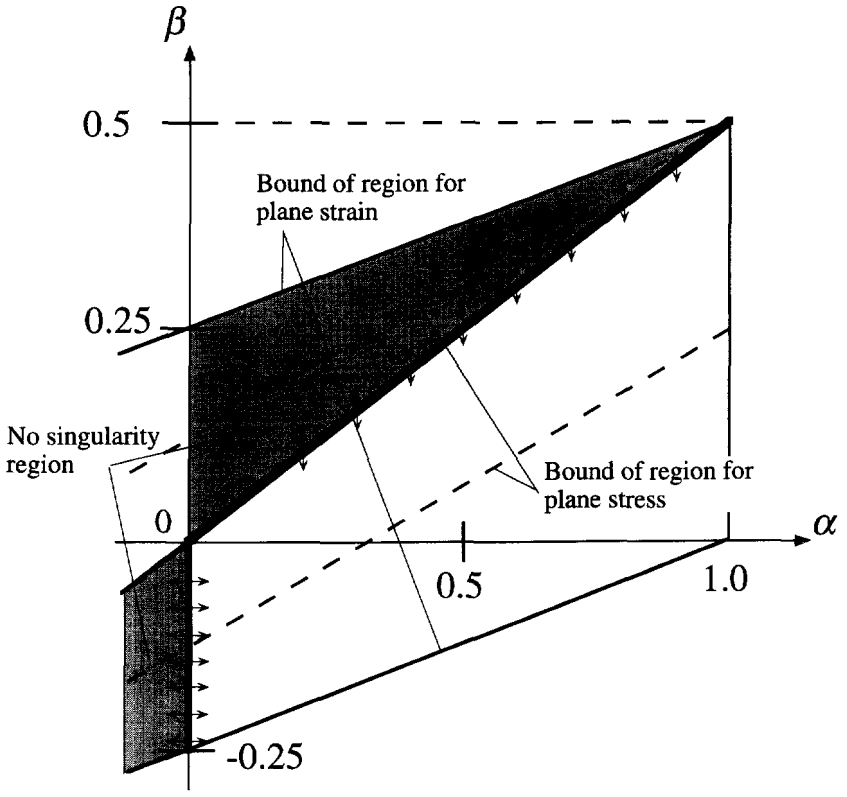

Fig. 21. Searching direction of pairs, α and β, yielding $\lambda = 0$ on Dundurs' composite plane.

joints. Further analyses are required to extend the present results to another configuration of joints.

3. CONCLUSION

We investigated the stress fields around the vertex of three-dimensional dissimilar materials using the boundary element method with Rongved's fundamental solution, which is satisfied with the boundary conditions at the interface. The order of stress singularity along a singularity line; intersection of a bonded plane with a free surface, varies from the value in plane strain to that in plane stress approaching the other free-surface side. The order of stress singularity at the vertex in the spherical coordinate system with an origin at the vertex rises when the stress singularity fields occur in the result of two-dimensional analysis. The order of singularity was also affected by a variation of the vertex angle between two free-surface sides, even if the pairs of material property and edge angles of the joint were fixed. As a result, the order increases with a decrease in the vertex angle and the joint with a small vertex angle fails easily. Finally, the bound on the α-β plane of Dundurs composite parameters diminishing the stress singularity in the three-dimensional stress state varied little in comparison with that deduced from the two-dimensional analysis except for a common domain of the α-β plane for plane strain and plane stress. Hence, we consider that the results in the two-dimensional analysis can be utilized for reducing the stress concentration occurring in the three-dimensional joints.

Acknowledgements—I thank Akira Fujiishi and Satoru Matsuda in the graduate school of Nagaoka University of Technology for performing the calculations of this investigation. Furthermore, I thank Professor Masataka Kobayashi at Nagaoka Technical College and Ikuo Ihara at Nagaoka University of Technology for their kind suggestions and discussion.

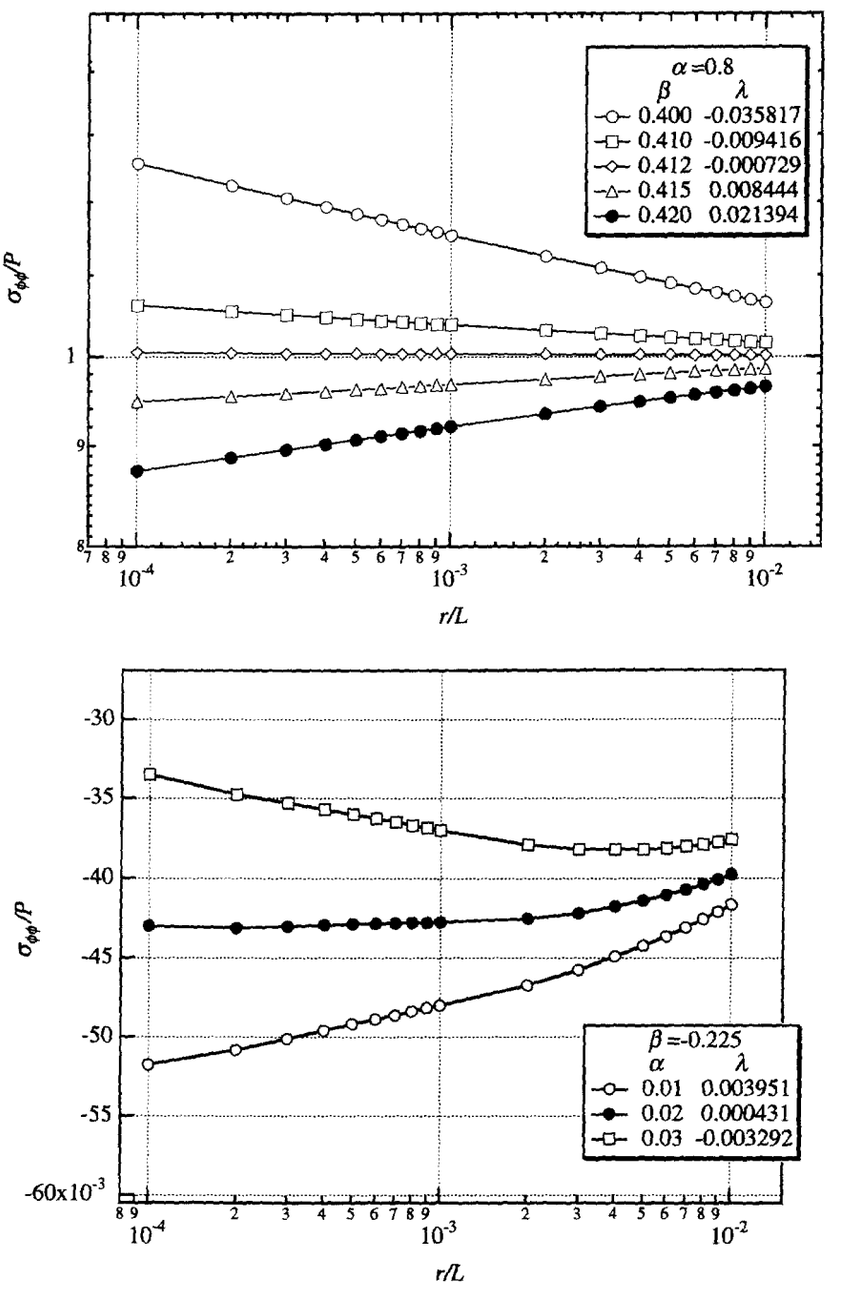

Fig. 22. Examples of distribution of dimensionless stress, $\sigma_{\phi\phi}/P$, in searching in Dundurs' parameters yielding $\lambda = 0$. (a) Distribution for several values of β at $\alpha = 0.8$. (b) Distribution for several values of α at $\beta = -0.225$.

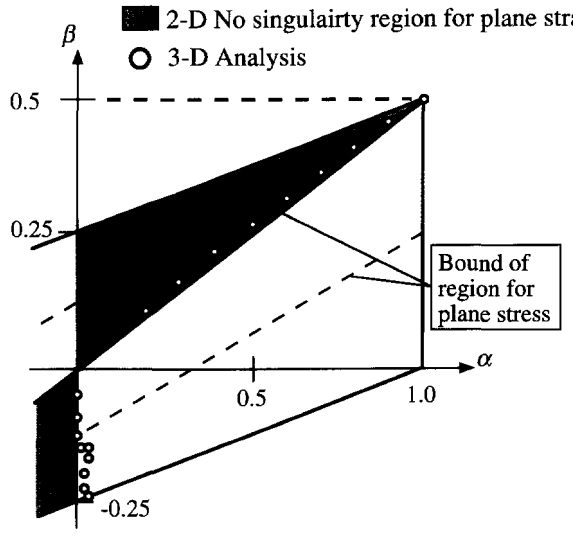

Fig. 23. Bound yielding no stress singularity plotted on Dundurs' parameters plane.

REFERENCES

Barsoum, R. S. (1988). Theoretical basis of the finite element iterative method for the eigenvalue problem in stationary cracks. *Int. J. Num. Methods Engng* **26,** 531–539.

Bazant, Z. P. and Estenssoro, L. F. (1979). Surface singularity and crack propagation. *Int. J. Solids Struct.* **15,** 405–426.

Benthem, J. P. (1977). State of stress at the vertex of a quarter-infinite crack in a half-space. *Int. J. Solids Struct.* **13,** 479–491.

Benthem, J. P. (1980). The quarter-infinite crack in a half space; alternative and additional solutions. *Int. J. Solids Struct.* **16,** 119–130.

Bogy, D. B. (1968). Edge-bonded dissimilar orthogonal elastic wedges under normal and shear loading. *J. Appl. Mech.* **35,** 460–466.

Bogy, D. B. (1970). On the problem of edge-bonded elastic quarter-planes at the boundary. *Int. J. Solids Struct.* **6,** 1287–1313.

Bogy, D. B. (1971a). Two-edge bonded elastic wedges of different materials and wedge angles under surface tractions—2. *J. Appl. Mech.* **38,** 377–386.

Bogy, D. B. (1971b). On the plane elastostatic problem of a loaded crack terminating at a material interface. *J. Appl. Mech.* **38,** 911–918.

Cook, T. S. and Erdogan, F. (1972). Stresses in bonded materials with a crack perpendicular to the interface. *Int. J. Engng Sci.* **10,** 677–697.

Dempsey, J. P. and Sinclair, G. B. (1979). On the stress singularities in the plane elasticity of the composite wedge. *J. Elasticity* **9,** 373–391.

Dundurs, J. (1969). Discussion of edge-bonded dissimilar orthogonal elastic wedges under normal and shear loading. *J. Appl. Mech.* **36,** 650–652.

Fenner, D. N. (1976). Stress singularities in composite materials with an arbitrarily oriented crack meeting an interface. *Int. J. Fracture* **12,** 705–721.

Ghahremani, F. A. (1991). Numerical variational method for extracting 3D singularities. *Int. J. Solids Struct.* **27,** 1371–1386.

Ghahremani, F. and Shih, C. F. (1992). Corner singularity of three-dimensional planar interface cracks. *J. Appl. Mech.* **59,** 61–68.

Hein, V. L. and Erdogan, F. (1971). Stress singularities in a two-material wedge. *Int. J. Fract. Mech.* **7,** 317–330.

Koguchi, H., Hino, T., Kikuchi, Y. and Yada, T. (1994). Residual stress analysis of joints of ceramics and metals. *Exp. Mech.* **34,** 116–124.

Koguchi, H., Inoue, T. and Yada, T. (1995). Stress singularity in three-phase bonded structure. Submitted to *J. Appl. Mech.*

Li, Y., Koguchi, H. and Yada, T. (1992). Investigation of method of stress relaxation around the apex of ceramics-metal bonded structure (consideration of shape effect of apex in three dimensional dissimilar materials). *Trans. Japan Soc. Mech. Engng* **58,** 1417–1423.

Pageau, S. S. and Biggers, S. B., Jr. (1995). Finite element evaluation of free-edge singular stress fields in anisotropic materials. *Int. J. Engng Sci.* **38,** 2225–2239.

Pageau, S. S., Joseph, P. F. and Biggers, S. B. (1994). The order of stress singularities for bonded and disbonded three-material junctions. *Int. J. Solids Struct.* **31,** 2979–2997.

Rongved, L. (1955). Force interior to one of two joined semi-infinite solids. In *Second Midwestern Conf. Solid Mechanics*. pp. 1–13.

Theocaris, P. S. (1974). The order of singularity at a multi-wedge corner of a composite plate. *Int. J. Engng Sci.* **12,** 107–120.

Thompson, T. R. and Little, R. W. (1970). End effects in a truncated semi-infinite cone. *Quart. J. Mech. and Applied Math.* **XXIII,** 185–195.

Williams, M. L. (1952). Stress singularities resulting from various boundary conditions in angular corners of plates in extension. *J. Appl. Mech.* **19**, 526–528.
Yang, Y. Y. and Munz, D. (1994). Determination of the regular stress term in a dissimilar materials joint under thermal loading by the Mellin transform. *J. Themal Stresses* **17**, 321–336.

APPENDIX

The fundamental solution for the two-phase materials is derived by employing the relationship of Papkovich-Neuber:

$$2GU_{ij} = (\kappa+1)\Phi^j_j - (x_k\Phi^j_k + \Psi^j)_j \tag{A1}$$

where Φ^j_j and Ψ^j represent the potential functions for a unit concentration force in the i-direction, and U_{ij} the displacement for the j-direction.

Solution of traction vector, $\mathbf{T}_{ij}$ can be derived by differentiating the displacement (A1)

$$\varepsilon_{jki} = \tfrac{1}{2}(U_{ik,j} + U_{ij,k}) \tag{A2}$$

and utilizing Hooke's law for isotropic materials and the normal unit vector, $\mathbf{n}_k$, as follows:

$$\begin{aligned}\mathbf{T}_{ij} &= \sigma_{jki}\mathbf{n}_k \\ &= G\left(2\varepsilon_{jki} + \frac{3-\kappa}{\kappa-1}\varepsilon_{lli}\delta_{jk}\right)\mathbf{n}_k.\end{aligned} \tag{A3}$$

Here the values of moduli G and κ for the region where the observation point exists are used in the analysis. The potential functions in the case where a unit concentration force acts at a point $P(0, 0, z_0)$ and the bonded plane is at $z = 0$, are presented as follows:

For the z-direction force:

when an observation point is located in the region I;

$$\begin{aligned}\Phi^3_z &= \frac{1}{2\pi(\kappa_1+1)}\left\{\frac{1}{R_1} + A\kappa_1\frac{1}{R_2} + 2A|z_0|\frac{z+|z_0|}{R_2^3}\right\} \\ \Psi^3 &= \frac{1}{2\pi(\kappa_1+1)}\left\{-|z_0|\frac{1}{R_1} - A\kappa_1|z_0|\frac{1}{R_2} + \tfrac{1}{2}(A\kappa_1^2 - B)\log(R_2+z+|z_0|)\right\}\end{aligned} \tag{A4}$$

when an observation point is located in the region II;

$$\begin{aligned}\Phi^3_z &= \frac{1-B}{2\pi(\kappa_1+1)}\frac{1}{R_1} \\ \Psi^3 &= \frac{1}{2\pi(\kappa_1+1)}\left\{-(1-A)|z_0|\frac{1}{R_1} + \tfrac{1}{2}[(1-A)\kappa_1 - (1-B)\kappa_2]\log(R_1 - z + |z_0|)\right\}\end{aligned} \tag{A5}$$

For the x-direction force:

when an observation point is located in the region I;

$$\begin{aligned}\Phi^1_x &= \frac{1}{2\pi(\kappa_1+1)}\left\{\frac{1}{R_1} + S\frac{1}{R_2}\right\} \\ \Phi^1_x &= \frac{1}{2\pi(\kappa_1+1)}\left\{(A\kappa_1 - S)\frac{x}{R_2(R_2+z+|z_0|)} - 2A|z_0|\frac{x}{R_2^3}\right\} \\ \Psi^1 &= \frac{1}{2\pi(\kappa_1+1)}\left\{-\tfrac{1}{2}(A\kappa_1^2 + B - 2S\kappa_1)\frac{x}{R_2+z+|z_0|} + (A\kappa_1 - S)|z_0|\frac{x}{R_2(R_2+z+|z_0|)}\right\}\end{aligned} \tag{A6}$$

when an observation point is located in the region II;

$$\begin{aligned}\Phi^1_x &= \frac{T}{2\pi(\kappa_1+1)}\frac{1}{R_1} \\ \Phi^1_z &= -\frac{1-B-T}{2\pi(\kappa_1+1)}\frac{x}{R_1(R_1 - z - |z_0|)}\end{aligned}$$

$$\Psi^{1} - \frac{1}{2\pi(\kappa_1+1)}\left\{-\tfrac{1}{2}[(1-A\kappa_1)+(1-B-2T)\kappa_2]\frac{x}{R_1-z+|z_0|}\right.$$
$$\left.+(1-A-T)|z_0|\frac{x}{R_1(R_1-z-|z_0|)}\right\} \tag{A7}$$

where

$$R_1 = \sqrt{x^2+y^2+(z-z_0)^2}$$
$$R_2 = \sqrt{x^2+y^2+(z+z_0)^2}$$
$$A = \frac{1-\Gamma}{1+\kappa_1\Gamma}$$
$$B = \frac{\kappa_2-\kappa_1\Gamma}{\kappa_2+\Gamma}$$
$$S = \frac{1-\Gamma}{1+\Gamma}$$
$$T = (1-s)\frac{\kappa_1+1}{\kappa_2+1}$$
$$\Gamma = \frac{G_{II}}{G_I} \tag{A8}$$
$$\kappa_i = 3-4\nu_i$$

The fundamental solutions for the y-direction force can be obtained by exchanging coordinates x and y.